INERTIAL ACCELERATION APPLICATION FOR WHEEL SLIP MEASUREMENT OF MOBILE ROBOTS

Daniel Szocs[(a)], Teodor Pană[(b)], Andrei Feneșan[(c)], Ioana Vese[(d)]

[(a), (b), (c), (d)]Technical University of Cluj-Napoca, Department of Electrical Drives and Robots

[(a)]Daniel.Szocs@edr.utcluj.ro, [(b)]Teodor Pana@edr.utcluj.ro, [(c)]Andrei.Fenesan@edr.utcluj.ro, [(d)]Ioana.Vese@edr.utcluj.ro

ABSTRACT

Smartphone three-axis acceleration sensors mounted on a mobile robot in conjunction with motor wheel encoders are used to determine wheel slip. Inertial acceleration is obtained by means of gravity compensation. Signal drift is observed when determining the vehicle speed by integrating the inertial acceleration data. A Kalman filter is used to correct noise from sensor data and attenuate the drift effect. Vehicle speed determined from acceleration sensor data is compared to wheel encoder data to determine wheel slip.

Keywords: sensor, filter, traction, robot

1. INTRODUCTION

Currently there is a wide spread of sensor equipped phones mainly used in game applications. In this paper, a three-axis acceleration sensor is mounted on top of a National Instruments Robotics Starter Kit™ mobile robot and uses the inertial component of the acceleration in conjunction with motor wheel encoders to determine wheel slip.

The principle of the wheel slip controller (Hori, Toyoda and Tsuruoka1997) for the Robotics Starter Kit is the following: when slip coefficient values exceed a certain value, the behavior of the active wheel is changed to increase grip. A PID controller imposes a rotational speed correction for the wheels and traction is regained. As opposed to other methods which require torque data (Cai 2010) or estimated tire force (Hong 2006), this method uses vehicle speed in conjuction with wheel speed to determine wheel slip.

The encoder speed is the speed measured by the optical encoder on the motor (Bräunl 2003). Sensor speed is the speed from the integrated acceleration sensor values. The sensitivity of the motor controller that commands the motor by translating PWM signal width to rotor speed is neglected in this model. This means the desired wheel speed and the encoder speed are considered to have the negligible differences. This is not true for small values of desired wheel speed, where small PWM command values are unable to determine motor spin.

A model of the vehicle is generated in MATLAB/Simulink™ and slip is simulated. Raw acceleration data is calibrated for amplitude and offsets that are dependent on the orientation of the accelerometer. Euler angles are used to determine gravitational acceleration. Inertial acceleration is extracted from the raw data by removing the gravitational component. A Kalman filter is used to smooth out the signal. Speed is obtained by integrating inertial acceleration. Wheel slip is measured using the speed data from inertial acceleration and wheel speed from the encoders.

2. TRACTION CONTROL METHODS

Traction control can be classified into the following: longitudinal control improves adhesion by controlling the traction force, and lateral control of yaw by varying the steering angle. Recently a lot of electric vehicles have been developed, mainly hybrid models using both electric and fossil fuel energy. The main catalyst for the development of electric vehicles is to solve current energy and environmental issues caused by combustion engine vehicles (ICV). Electric motors have instantaneous high torque, quickly and precisely controlled as opposed to internal combustion engines.

One paper (Hori, Toyoda and Tsuruoka1997) proposes two methods for traction control for electric vehicles: "Model Following Control (MFC)" and "Optimal Slip Ratio Control". In the MFC, the actual speed is compared to the simulated speed output of the vehicle model; motor torque is reduced and traction is increased.

The side force has a maximum value when λ=0 and decreases rapidly for bigger λ. Sudden decrease of road friction causes λ to increase, the side force decreases as well. This has serious consequences: front wheel drive cars drift, rear wheel drive cars spin, and four wheel drive cars drift and rotate.

In the Optimal Slip Ratio Control, the road condition estimator decides the optimal slip ratio, the slip ratio controller uses this information to control the torque and obtain the desired slip ratio.

Slip ratio is defined as:

$$\lambda = \frac{(V_W - V)}{V_W} \quad (1)$$

where V_W is wheel speed and V is vehicle speed.

The kinematic equations of the wheel and of the vehicle are as follow:

$$(F_m - F_d)/(M_W \cdot s) = V_W \quad (2)$$

$$F_d/(M \cdot s) = V \quad (3)$$

where F_m is motor torque (force equivalent); F_d is friction force; M_W is wheel inertia (mass equivalent); M is vehicle weight.

The vehicle body can be seen as one inertia system with equivalent inertia moment J, by introducing the slip ratio λ,

$$J = J_W + M \cdot r^2(1 - \lambda) \quad (4)$$

where J_W, M and r are the shaft inertia moment, vehicle weight and tire radius.

2.1. Wheel Slip Ratio Control For Electric Vehicle

The principle of the wheel slip controller for the electric vehicle prototype Robotics Starter Kit is the following: when slip coefficient values exceed a certain value, the behavior of the active wheel is changed to increase grip. A PID controller imposes a rotational speed correction for the wheels and traction is regained (Fig. 1).

The desired wheel speed is the command for the rotational speed of the wheel. The encoder speed is the speed measured by the optical encoder on the motor (Bräunl 2003). Sensor speed is the speed from the integrated acceleration sensor values. The sensitivity of the motor controller that commands the motor by translating PWM signal width to rotor speed is neglected in this model. This means the desired wheel speed and the encoder speed are considered to have the negligible differences. This is not true for small values of desired wheel speed, where small PWM command values are unable to determine motor spin.

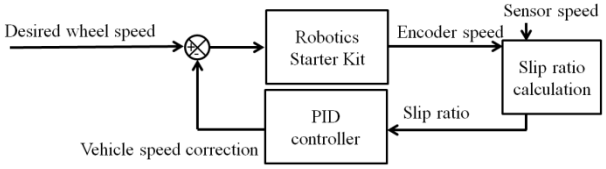

Figure 1: Wheel Slip Ratio Controller for the Robotics Starter Kit Electric Vehicle Prototype

3. ROBOT COMPONENTS AND FUNCTIONALITY

For the purpose of modeling the behavior of an electric automobile, a four-wheeled robot was used. Two motors drive the wheels by means of reduction gears so that the rotational speed at the wheels is half the speed of the spinning DC motor shaft. All the electrical components are placed on a solid plane attached to the robot chassis. An ultrasonic sensor mounted on a servomotor serves for orientation purposes. The robotic platform NI Robotics Starter Kit is comprised of a sbRIO9631™ embedded device with AI, AO, DIO, 1M Gate FPGA. The programming is realized using the LabVIEW™ graphical development environment, programs are compiled using Xilinx™ tools and written to field programmable-gate arrays on NI reconfigurable I/O hardware through the Ethernet port.

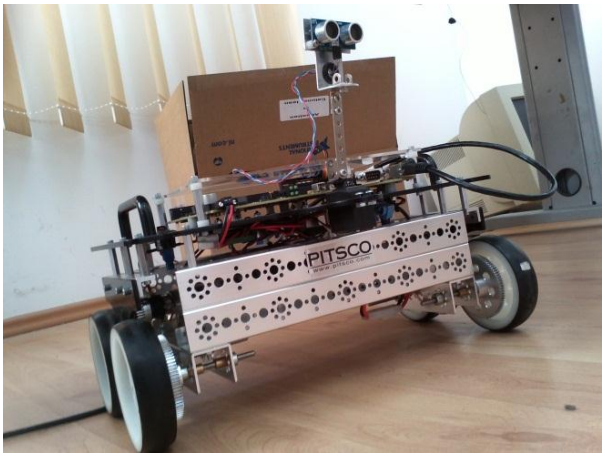

Figure 2: Robotic Starter Kit Electric Vehicle Prototype Platform – Photo Taken Inside the PhD Office at National Instruments Cluj-Napoca Headquarters

Digital I/O Port P2 is connected to a mezzanine board, which further connects to the motors controller, encoder sensors, ultrasonic sensors and its servomotor controller. A 12 V, 3000 mAh Ni-MH battery serves as a power supply and a 12 V - 24V DC converter adjusts the power requirements for the sbRIO9631™. Two DC motors are powered and controlled by a dual DC motor controller. Rotation is sent to the wheel using a 1/2 gear ratio.

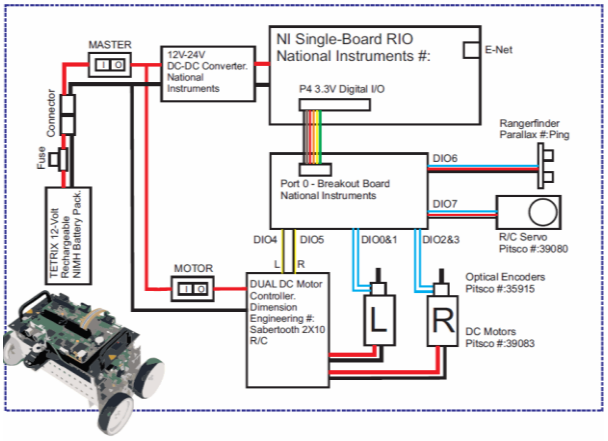

Figure 3: Labview Robotics Starter Kit Block Diagram

Motors are two RC servo controlled continuously rotating motors. A PWM signal is generated to control the motors: 1000(μs) pulse width corresponds to full backward speed, 1500(μs) to motor stop and 2000(μs) to full forward speed. Only the pulse width affects the speed, not the amplitude or the frequency. The duty

cycle and current amperage affect torque. Amplitude of current dictates the amplitude of torque, and the duty cycle affects the jerkiness of the torque. For example, a 0.5 duty cycle means half of the time torque will be one hundred percent and half of the time it will be zero. Frequency of the signal affects the command rate, or how often one can change the command in a period of time.

The signal command is generated through ports DIO4 and DIO5 for the left and right motor respectively. Note that the motors have opposite motor movement, due to the opposite physical position of the motors shaft, this affects the PWM command.

Rotary optical encoders, one for each of the two motors, give absolute position feedback with 400 position increments. Data is sent through DIO0, DIO1 for the left motor and DIO2, DIO3 for the right.

In LabVIEW™, forward and angular velocity are transformed into left and right wheel velocities. A differential steer and fixed wheel frame is defined, wheel radius, wheel base and ratio are set.

4. SLIP SIMULATION IN MATLAB/SIMULINK™

The vehicle is modeled using equations (1), (2), (3) and the Matlab/Simulink graphical programming environment. From the vehicle and wheel model as well as a given motor torque, we determined wheel drift.

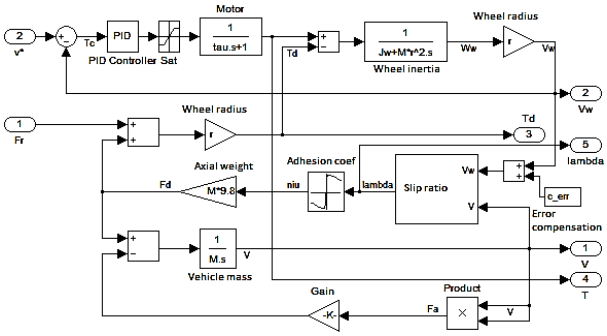

Figure 4: Vehicle Model Structure in Simulink. Generates Wheel and Vehicle Speed and Determines Slip Ratio

The following parameters have been defined:

Table 1. Wheel Slip Simulation Parameters

Simulation parameter name	Value(unit)
resistant wheel friction force, F_r	6.125(Nm)
wheel radius, r	0.0508(m)
wheel inertia moment, J_w	0.00077(kg·m^2),
vehicle mass, M	3.6(kg)
air density, ρ_a	1.205(kg⁄m^3)
air friction coefficient, c_{fa}	0.3
front vehicle area, A	0.035(m^2).

From 0 to 800(ms) there is an acceleration interval where the vehicle accelerates to the maximum speed: 0.3(m⁄s) (Fig. 5) and the torque is at maximum constant value (Fig. 6).

Speed is constant from 800 to 1000(ms); motor torque decreases and has same value as resistant torque. Until the 1550(ms) mark, the vehicle brakes and stops, motor torque is negative and less than resistant torque. Total simulation time is two seconds.

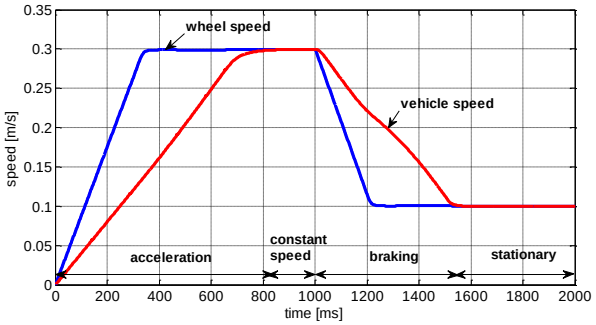

Figure 5: Wheel and Vehicle Speed Characteristic Simulation in Simulink; Four Phases of Movement: Acceleration, Constant Speed, Braking and Stationary

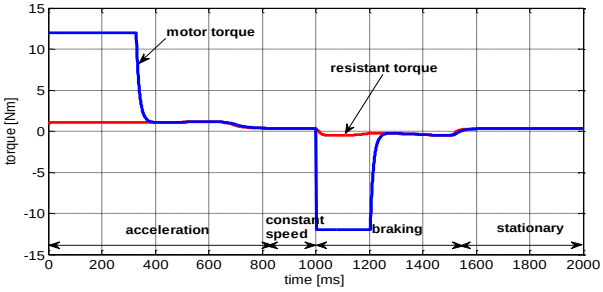

Figure 6: Motor and Resistant Torque Characteristic Simulation in Simulink

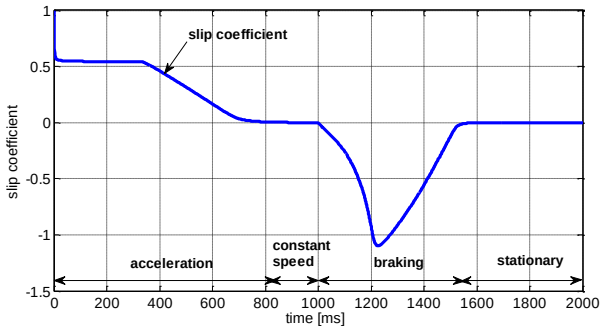

Figure 7: Slip Coefficient Characteristics Simulation in Simulink

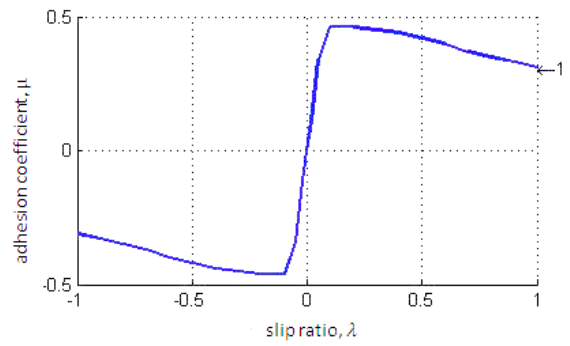

Figure 8: Adhesion Coefficient as a Function of Slip

ratio, by interpolating discrete values in a reference table.

In figure 8, the μ−λ characteristic used in the simulation is generated by interpolating discrete values in a reference table. Wheel speed, vehicle speed, motor torque and resistant torque are the main parameters defining the vehicle behavior. Using (1), slip coefficient is found (Fig. 7).

5. SENSOR SIGNAL ACQUISITION AND CONDITIONING

Sensors are provided from an LG P970™ smartphone and data is transmitted via Bluetooth. The phone contains a gyroscope, an accelerometer, a magnetic compass sensor.

Currently acceleration sensor, magnetic sensor and orientation information is available to the LabVIEW™ environment, using an Android™ application that transmits wireless Bluetooth sensor information.

Raw acceleration data contains the gravitational acceleration as well as inertial linear acceleration. From the acceleration data, the gravitational component is removed by means of orientation compensation and the result is linear acceleration. Gravitational acceleration has a constant value as long as the sensor moves parallel to the ground plane; inertial acceleration or linear acceleration along one axis is the acceleration generated by movement.

5.1. Amplitude Calibration for Gravitational Acceleration

Consider a stationary accelerometer, oriented with one of its axis in the vertical place, so the measured values for each axis must read +g for the positive direction of the down pointing oriented axis, or -g for the negative axis pointed in the same direction. After measurements are done using the accelerometer, there is a noticeable deviation from the gravitational constant. Local gravitational acceleration is considered, obtained from latitude and altitude values (Boynton, 2001).

Furthermore, the amount of deviation can vary from one accelerometer device to another. Calibration will result in three linear equations, one for each axis. The equations can then be applied to correct the acceleration values and are unique for each device.

Orientation of the device is done using the right hand rule, considering the z-axis perpendicular to the mobile device's surface and oriented downwards, the y-axis is aligned to the width and oriented to the right side, the x-axis is aligned to the length of the device and oriented upwards, where the start button resides. The axis system is considered fixed to the mobile device.

This method is based on measurements in static conditions, with the accelerometer at rest and with the read axis oriented vertically. One hundred discrete values are taken from the axis that is calibrated. After the values have been collected, the device is rotated 90 degrees and the measurements are repeated for the next axis. The process is repeated until the device has done a full rotation.

By using values in the acquired measurement database, an average and standard deviation of the samples is determined for positive and negative values of acceleration.

$$\overline{a_x} = \frac{\sum_{j=1}^{n} a_{xj}}{n} \tag{5}$$

where a_x represents the arithmetic mean of acceleration values for the x-axis, a_{xj} are values of the x-axis acceleration, and n represents the number of discrete values of the digital signal for acceleration.

Standard deviation of the sample is defined:

$$\sigma_x = \sqrt{\frac{1}{n-1}\sum_{j=1}^{n}(a_{xj} - \overline{a_x})^2} \tag{6}$$

It is a measure of signal quality; it describes the absolute value of deviation from the mean value.

For each axis, the "two point formula" is used to determine the slope and the intercept, considering two points of coordinates (mean value for negative x-axis, negative value of gravitational acceleration). By applying the two point formula, one equation for each axis results in the form of:

$$y = mx + n \tag{7}$$

where m is the slope and n is the intercept.

Slope is determined with the formula:

$$m = \frac{Y_2 - Y_1}{\overline{a_{x+}} - \overline{a_{x-}}} \tag{8}$$

where m is the slope, Y_2=9.80678 is the value for local gravitational acceleration, $Y1 = -Y_2$, a_{x+} and a_{x-} are mean values of sample acceleration for positive x-axis and negative x-axis, respectively. The slope gives a value of the scale between the compensated and not compensated signal.

The intercept n aligns the mean value of acceleration to the nominal value of acceleration, resulting in a signal that is in the ±9.80678(m/s^2) interval.

$$n = m\overline{a_{x+}} - Y_2 \tag{9}$$

The corrected value of the x-axis acceleration, after calibration, is: $a_{xcor} - a_{xe}\ (m/s^2)$

$$a_{xcal1} = ma_x - n \tag{10}$$

Value for acceleration at horizontal orientation is given correctly from the accelerometer, but after calibration, an error is introduced because of the n parameter. Also, positive and negative semi-periods have different amplitudes. For this reasons, the method of calibration will be applied separately on each semi-period, one of the two points will be considered the origin of the axis.

After calibration, the values for ±90 degrees are identical to the Euler determined values. This is a necessary condition for calibration, but it is not sufficient. After further examination, it seems the calibrated signal still presents a difference relative to the ideal signal. Other measurement values for this method of calibration in semi-periods will be presented in the next subchapter.

5.2. Gravitational Calibration in Quarter-Periods

The δ_x difference from the ideal value has a double sinusoidal shape when it is represented as a function of orientation angle θ, as presented in figure 9.

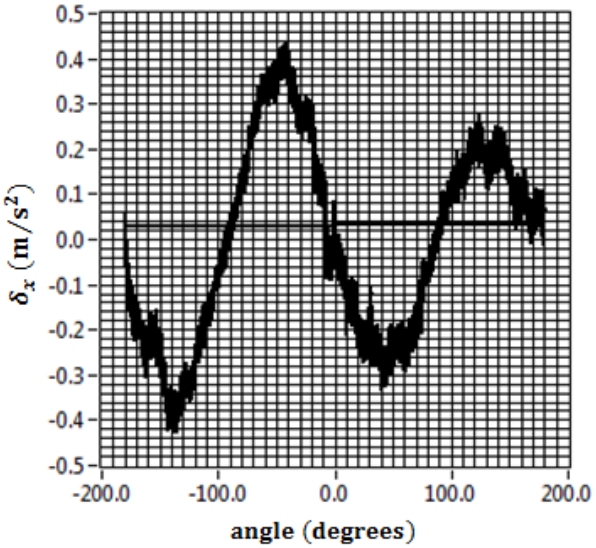

Figure 9: Shape of the Semi-Period Calibrated Gravitational Acceleration Deviation from the Euler Determined Gravity Component

$$\delta_x = a_{xcal1} - a_{xe} \tag{11}$$

Readings are done for δ_x at ±45 and ±135 degree values. An additional calibration signal is defined:

$$a_{xcal2} = \delta_{xqp}\sin(2\theta), \tag{12}$$

Where

$$\delta_{xqp} = \begin{cases} \delta_{x-135}, -180 < \theta \leq -90; \\ -\delta_{x-45}, -90 < \theta \leq 0\,; \\ \delta_{x+45}, 0 < \theta \leq 90\,; \\ -\delta_{x+135}, 90 < \theta \leq 180. \end{cases} \tag{13}$$

$$a_{xcal} = a_{xcal1} - a_{xcal2} \tag{14}$$

Values are compared for the uncompensated signal and the compensated signals in the following table:

Table 2. Values For X-Axis Gravity Components at Different Angles and Calibration Methods

θ [degrees]	-135	-45	45	135
$\overline{a_x}$ (m/s^2)	6.56	7.24	-7.32	-6.73
$\overline{a_{xcal1}}$ (m/s^2)	6.70	7.35	-7.26	-6.66
$\overline{a_{xcal}}$ (m/s^2)	6.92	6.93	-6.91	-6.94
$\overline{a_{xe}}$ (m/s^2)	6.93	6.94	-6.93	-6.93

where $\overline{a_x}$ is the mean value of the uncompensated gravitational acceleration, $\overline{a_{xsp}}$ is the mean compensated value for semi-periods, $\overline{a_{xds}}$ is the mean double sinus value, $\overline{a_{xe}}$ is the mean Euler derived acceleration value. Experimental measurements have been done for ±45 and ±135 degrees θ angle orientation.

After the signal is calibrated at ±45 and ±135 grade, it has a ±0.01(m/s^2) error of the calibration points and overall the error is ±0.15(m/s^2) as seen in figure 10. Large variations of error for a particular angle value are due to the fact that measurements were taken by manually rotating the accelerometer device and inertial acceleration has been added to the signal.

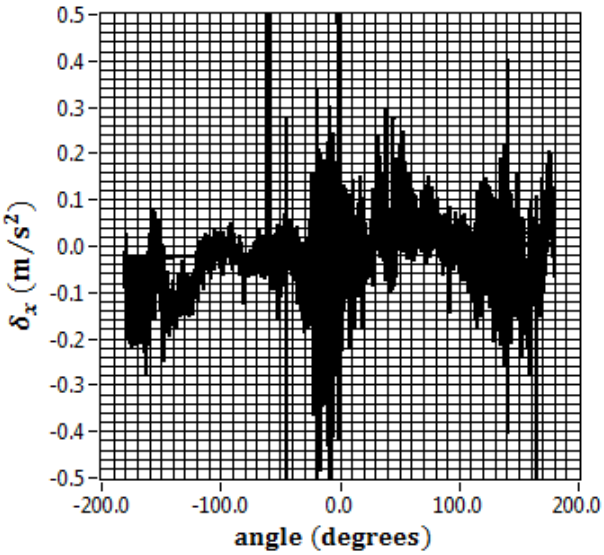

Figure 10: Shape of the Quarter-Period Calibrated Gravitational Acceleration Deviation.

5.3. Determining Inertial Acceleration

The Euler angles are a set of three angles that describe a number of three consecutive rotations around predefined axes. The mobile device that contains an accelerometer, also gives Euler angle values for an *XYZ* type rotation. It has a particular condition, which is that the final orientation is generated using only the first two rotations, meaning the rotation around *z* is considered null.

Rotation matrices describe rotation around a particular axis. By multiplying them, we get a generalized rotation matrix that is comprised of a rotation around *x* by φ degrees, then around *y* by θ degrees and lastly around *z* by ψ degrees.

$$R_{XYZ}=R_x(\psi)R_y(\theta)R_z(\varphi) \tag{15}$$

The generalized form is:

$$R_{XYZ} = \begin{bmatrix} R_{00} & R_{01} & R_{02} \\ R_{10} & R_{11} & R_{12} \\ R_{20} & R_{21} & R_{22} \end{bmatrix} \quad (16)$$

where

$$\begin{cases} R_{00} = \cos\theta\cos\varphi \\ R_{01} = -\cos\theta\sin\varphi \\ R_{02} = \sin\theta \\ R_{10} = \cos\psi\sin\varphi + \cos\varphi\sin\psi\sin\theta \\ R_{11} = \cos\psi\cos\varphi - \sin\psi\sin\theta\sin\varphi \\ R_{12} = -\cos\theta\sin\psi \\ R_{20} = \sin\psi\sin\varphi - \cos\psi\cos\varphi\sin\theta \\ R_{21} = \cos\varphi\sin\psi + \cos\psi\sin\theta\sin\varphi \\ R_{22} = \cos\psi\cos\theta \end{cases} \quad (17)$$

By multiplying the rotation matrix with the gravitational vector, we get the projections of the gravitational acceleration on the three axes.

$$R_{XYZ} \times \begin{bmatrix} 0 \\ 0 \\ g \end{bmatrix} = \begin{bmatrix} g_x \\ g_y \\ g_z \end{bmatrix} \quad (18)$$

Now that the gravitational acceleration has been determined, we apply the difference between the accelerometer readings and gravitational acceleration to obtain pure inertial acceleration. This is also called gravity compensation.

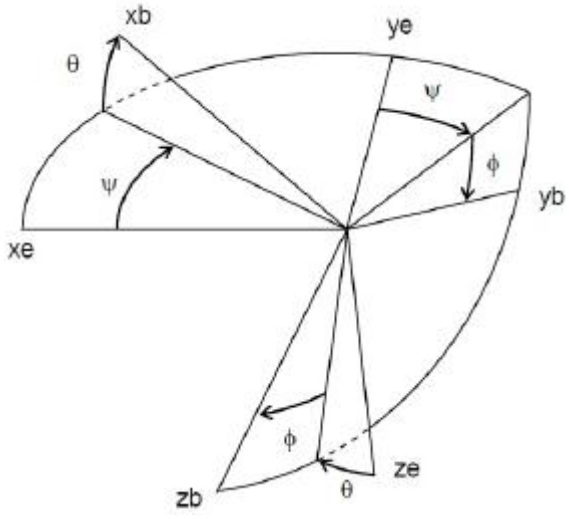

Figure 11: Euler Angles for a Fixed Earth and a Fixed Body Frame of Reference

Prior to compensation, the accelerometer is calibrated for latitude and altitude influences (Boynton, 2001), also the amplitude is calibrated using the two point formula:

$$a_{xcal} = ma_x - n \quad (19)$$

where *m* is the slope and *n* is the intercept.

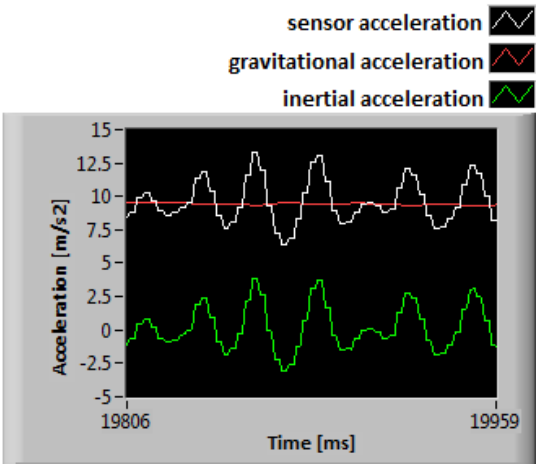

Figure 12: Sensor Acceleration in the *X* Direction, Contains Raw Sensor Data (Combined Acceleration); Gravitational Component and Inertial Component

In figure 12, the mobile device was oriented with the *x* axis oriented perpendicular to the ground and pointing downward. The variations in acceleration are caused by moving the phone up and down along its x axis. *Sensor acceleration* is the raw data from the sensor; *gravitational acceleration* has a constant value as long as the sensor moves parallel to the ground plane; *inertial acceleration* or linear acceleration along one axis is the acceleration generated by movement.

5.4. Signal Noise Cancelation

To measure the robot state, i.e. the position, velocity or acceleration, sensors are used. Measurement is done by sampling data every period of time; measurements include errors determined by alignment, sensitivity, noise.

Low-pass filters give signals a smooth form, by removing short-term fluctuations and providing the desired long-term component.

For the sake of comparison, five filters have been tested: Kalman (Bizup 2004), Median, Butterworth, Chebyshev and Bessel. With the exception of the Kalman filter, the experiment results show they have little effect on small variation, the amplitude of the error remains the same and the filters introduce lag, probably from the extra time it takes to calculate the new values from raw data. The Kalman Filter proved to be the best at removing noise error, reducing it by an order of magnitude.

The Kalman filter is used to smooth the signal by removing noise. Small changes of linear acceleration in the cm/s^2 range are indistinguishable from the sensor error, so these are filtered out also. It is observable that the noise error is reduced by a factor of ten. Large variations, in the order of units of m/s^2 are not filtered out.

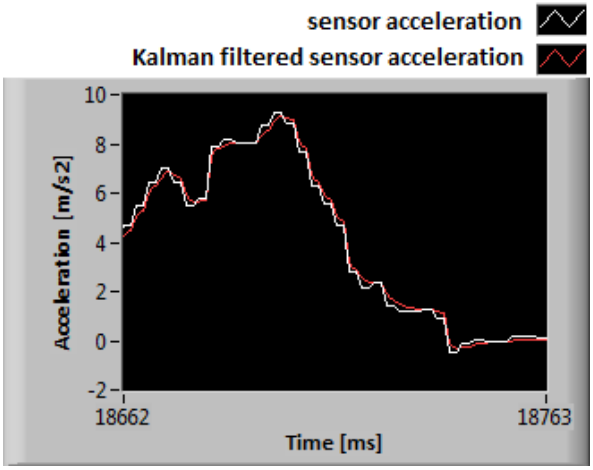

(A)

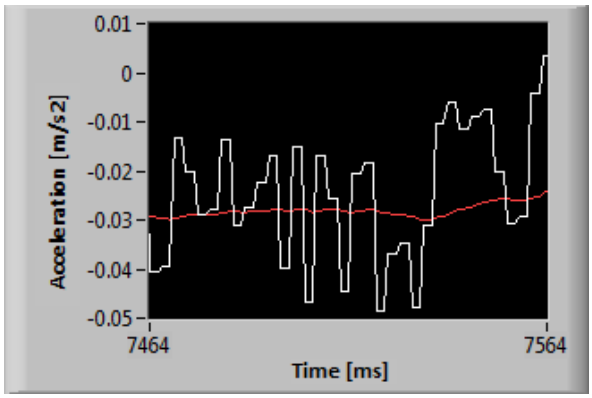

(B)

Figure 13: Measured Sensor Acceleration (m/s^2) and Kalman Filtered Data for Large (A) and Small (B) Variations

5.5. SPEED BY INTEGRATION

By integrating the linear acceleration along the *x* axis, linear speed results:

$$\int [a_x(t) + err_{n.x}(t)]\, dt = v_x(t) + coeff_{drift.x}(t) \quad (20)$$

An integration constant, C, is also added to the second term of the equation.

Integration of the acceleration samples is done point by point, dividing two small variations in one period of time. Last acceleration value is given at the beginning of the new period and measured again in the current. Subtracting the last value from the previous gives us a measure of acceleration in one period of time. Times values are also subtracted, present time from last period time. Shift registers are used for this purpose.

Initial conditions are v_{x0}=0 and t_0=0.

$$a_{x1} = v_{x1}/t_1 \quad (21)$$

$$a_{x2} = v_{x2} - v_{x1}/t_2 - t_1 \quad (22)$$

$$a_{xj} = (v_{xj} - v_{xj-1})/(t_j - t_{j-1}), for\ j \epsilon N \geq 1 \quad (23)$$

From (15), the value for v_{xj} is extracted:

$$v_{xj} = a_{xj}(t_j - t_{j-1}) + v_{xj-1} \quad (24)$$

$$v_{xj} = \Delta v_{xj} + v_{xj-1} \quad (25)$$

The raw inertial acceleration signal contains measurement errors in the range of ±0.02(m/s^2).

Drift is observed in figure 14 and is caused by integration of read errors $err_{n.x}$ (10). Although only speed measurements are required for our purpose, by further integrating the speed signal, the position can be obtained. The drift would further be amplified and the simulated signal value would drift quickly from the real value.

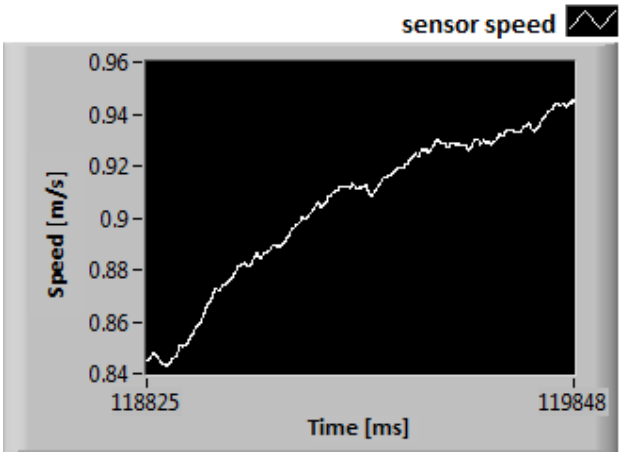

Figure 14: Sensor Speed Data Obtained by Integrating the Sensor Acceleration Data

6. WHEEL SLIP MEASUREMENT APPLICATION

Linear speed is obtained both from the sensor and encoders: the first one, by integrating the sensor linear acceleration and the second one from derivation of wheel motor position. In Figure 15 the vehicle accelerates until a constant speed of negative 0.3(rad/s) is achieved. Note that this is not reverse movement; the negative value is due to inverse position of the right motor with respect to the left motor; same shaft axis, opposite rotational direction.

Wheel slip is determined from equation (1), vehicle speed is determined from inertial acceleration integration and wheel speed is obtained from the digital encoders mounted at each motor axis.

The first period of positive wheel slip for the vehicle lasts for 15(ms), until the 65545(ms) mark: λ=0.8 The second one is shorter, only lasts 5(ms) until the 65550(ms) mark with larger slip: λ=1.5. Negative slip (wheel block) is observed from 65550 to 65560(ms), λ=–0.24. After this point in time, slip stabilizes to a value close to zero.

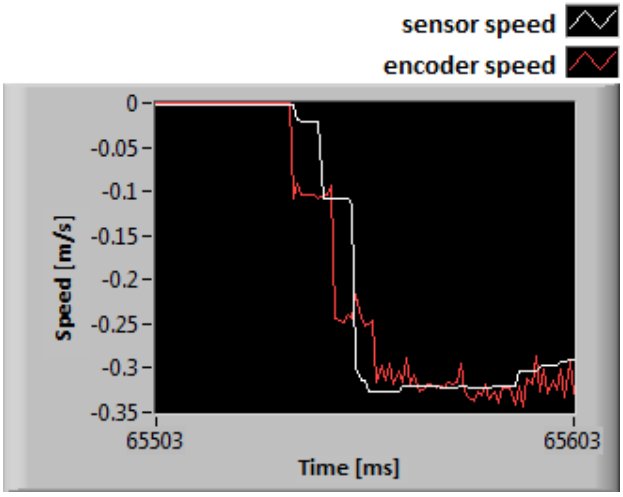

Figure 15: Measured Sensor and Encoder Speed. Acceleration Phase is Shown.

Using the wheel slip data in a closed loop, wheel control can be obtained. Depending on the position of the slipping wheel, corrections can be made to the slipping wheel or any of the other wheels to correct the behavior and regain grip.

7. CONCLUSIONS

Theoretical absolute value for gravitational acceleration is calibrated for latitude and altitude, signal amplitude is calibrated in semi-periods and further calibration is done in quarter-periods.

Gravitational component is determined using Euler angles. It then must be removed from raw acceleration sensor data to obtain inertial acceleration.

Noise errors accumulate during integration, the Kalman filter reduces noise by a factor of ten.

Inertial acceleration data is transformed into vehicle speed data and compared to wheel speed to measure wheel slip.

Slip is very small in value and time for the Robotics Starter Kit. To better visualize the wheel slip and the effect of the slip control, changes are proposed. In the future, the slip coefficient value will be forced to rise by changing the road surface to one with low adhesion coefficient and by changing the wheel tire surface with a more slippery one, like plastic instead of rubber.

REFERENCES

Bizup, D.F., 2004. A generalized acceleration model for Kalman filter trackers. *Proceedings of the Thirty-Sixth Southeastern Symposium on System Theory*, pp. 31-35, September 27, Atlanta, Georgia, USA.

Boynton, R., 2001. Precise Measurement of Mass, Proceedings of the 60th Annual Conference of the Society of Allied Weight Engineers, pp.4-8, May 21-23, Arlington, Texas, USA.

Bräunl, T., 2003. Embedded Robotics, Berlin Heidelberg: Springer

Cai, Z., Ma, C., Zhao, Q., 2010. Acceleration-to-torque Ratio based Anti-skid Control for Electric Vehicles, *Proceedings of IEEE/ASME International Conference on Mechatronics and Embedded Systems and Applications (MESA)*, pp 577-581, July 15-17, Qingdao, ShanDong, China.

Hong, D., Yoon, P., Kang, H.J., Hwang, I., Huh, K., 2006. Wheel Slip Control Systems Utilizing the Estimated Tire Force. *Proceedings of the American Control Conference*, pp. 1-6. June 14-16, Minneapolis, Minnesota, USA.

Hori, Y., Toyoda, Y., Tsuruoka Y., 1997. Traction Control of Electrical Vehicle based on the Estimation of Road Surface Condition – Basic Experimental Results using the Test EV 'UOT Electric March'. *Proceedings of the Power Conversion Conference*, pp. 1-7, August 3-6 Nagaoka, Japan.

AUTHORS BIOGRAPHY

Szöcs Daniel is an electrical engineer and third year PhD candidate at the Technical University of Cluj-Napoca, Department of Electrical Machines and Drives. Research for the doctoral thesis was made at National Instruments Romania, the hardware basis for the research is the National Instrument Robotics Starter Kit. Research topics: direct-drive electrical vehicles, anti-slip control.

Fenești Andrei is an electrical engineer and second year PhD candidate. Research topics: direct-drive electrical vehicles, obstacle avoidance, trajectory control with LADAR and GPS technology.

Pană Teodor is head of the Department of Electrical Machines and Drives and professor of Microprocessor and Computer Systems, as well as two other digital control based courses at the Technical University of Cluj-Napoca, Faculty of Electrical Engineering and Research topics: vector control systems, electric vehicle drive control, industrial robots.

Vese Ioana is an electrical engineer and PhD at the Technical University of Cluj-Napoca, Department of Electrical Machines and Drives**.** Research topics: modeling and simulation of electrical machines, design, modeling and control of linear motors and actuators, design and control of small electric motors.